Construction and Building Materials 490 (2025) 142551

Contents lists available at ScienceDirect

Construction and Building Materials

journal homepage: www.elsevier.com/locate/conbuildmat

Finite element and experimental investigation of the inclined pull-out behavior of hooked-end steel fibers from carbon nanotube-reinforced ultra-high performance concrete

Hakan Çağlar

Faculty of Engineering and Architecture, Department of Civil Engineering, Kırşehir Ahi Evran University, Kırşehir, Turkey

ARTICLE INFO

Keywords:
Ultra-high performance concrete
Inclined pull-out
Hooked-end fibers
Carbon nanotubes
Bond strength
Cohesive zone model

ABSTRACT

This research investigates, both numerically and experimentally, the combined effects of carbon nanotube (CNT) and inclination on the pull-out performance of hooked-end steel fibers embedded in CNT-reinforced ultra-high performance concrete (UHPC). For numerical simulation, the finite element method (FEM) was employed using ABAQUS software, with modeling implemented based on cohesive zone theory (CZM). The mechanical properties of the CNT-reinforced UHPC, along with the CZM parameters, were derived from experimental testing across a range of CNT weight percentages (0 %, 0.1 %, 0.2 %, 0.4 %, and 0.6 %). These experimental tests included inclined pull-out tests of both straight and hooked-end steel fibers from UHPC specimens incorporating the aforementioned CNT concentrations. Following validation of the FEM results, a parametric study was conducted to estimate the influence of inclination angle and CNT content on the pull-out response, including peak pull-out force, slip at peak force, pull-out energy, and the extent of matrix spalling observed in each configuration. Results indicate that the inclusion of CNTs enhances the fiber-matrix bond, leading to improved pull-out resistance.

1. Introduction

Ultra-high performance concrete (UHPC) has garnered significant attention as a novel material in the construction and infrastructure industries due to its outstanding mechanical properties, including high compressive strength, enhanced durability, and adequate toughness [1–3]. However, the inherent brittleness of this concrete type poses a fundamental limitation to its structural applications. To address this challenge, the use of steel fibers, particularly hooked-end fibers, has been proposed as an effective solution for improving bond behavior and increasing energy absorption capacity. Furthermore, the incorporation of CNTs into the cementitious matrix can enhance the mechanical and microstructural properties of the concrete, leading to an improved fiber-matrix bond [4].

The adhesion between fibers and the concrete matrix is a crucial factor in improving the mechanical performance of fiber-reinforced cementitious composites [5–9]. This adhesion is influenced by various parameters, including fiber geometry, the strength and structure of the cementitious matrix, the amount and dispersion method of nanomaterials, and the fiber orientation angle within the concrete. Due to their end hooks, hooked-end fibers create a stronger mechanical interlocking mechanism compared to straight fibers, resulting in increased pull-out resistance [10–12]. Nanoparticles, due to their unique structural and functional properties, play a pivotal role in the advancement and transformation of various scientific and technological fields [13–18]. Moreover, the existence of CNTs in the cementitious matrix can increase the interfacial bond between fibers and concrete, thereby strengthening the adhesion behavior [19–21]. The fiber orientation angle is also a significant factor in the degree to which the fibers contribute to resisting tensile and shear stresses. Specifically, fibers with an inclined orientation, compared to vertical or horizontal fibers, exhibit a different failure mechanism and have a greater impact on crack behavior. Therefore, accurate analysis of the effects of these parameters on fiber adhesion can lead to the development of more advanced models for simulating fiber-matrix interaction, as well as the design of UHPC with optimized performance.

Various studies have investigated the pull-out response of fibers with different geometries in UHPC [22–24]. Zhang et al. [25] examined the effect of fiber shape (straight, hooked, corrugated) on adhesion and pull-out resistance and demonstrated that hooked fibers, due to mechanical interlocking, performed better in increasing the bond strength with the concrete matrix. Li et al. [26] used FEM to simulate the bond

E-mail address: c.hakan@ahievran.edu.tr.

https://doi.org/10.1016/j.conbuildmat.2025.142551
Received 25 March 2025; Received in revised form 27 June 2025; Accepted 1 July 2025
Available online 4 July 2025

between concrete and fibers and found that the fiber angle and length had a direct impact on the pull-out resistance. Lee et al. [27] also investigated the influence of CNTs on enhancing adhesion and improving the tensile behavior of concrete and found that combining CNTs with steel fibers led to improved bonding and increased concrete strength. Furthermore, Esmaeili et al. [28], in a comparison between different types of fibers, showed that hooked steel fibers required a greater pull-out force than straight and corrugated fibers and performed better in resisting cracking.

A comprehensive understanding of fiber pull-out behavior in UHPC is provided by the literature now under publication, emphasizing the intricate interactions between geometric, material, and environmental aspects [29–31]. A thorough evaluation of the impact of steel fiber type on the macroscopic response of UHPC is given by Yoo et al. [32], who compare the geometries of straight, hooked, twisted, and half-hooked fibers. Their methodical approach, which includes a variety of inclination angles that are indicative of the naturally random fiber orientation in UHPC, emphasizes how important mechanical interlocking is for improving tensile performance and pull-out resistance. The results highlight how crucial it is to take fiber geometry into account as a crucial design factor in order to maximize the mechanical behavior of UHPC. In their investigation of the temporal evolution of bond strength in UHPC, Krahl et al. [33] show how the fiber-matrix interface gradually develops over time. Their findings, which came from meticulously regulated pull-out experiments carried out at different ages and fiber inclination angles, show that curing time and bond strength development are exponentially related. This emphasizes how important proper curing conditions are to guaranteeing the long-term functionality and robustness of UHPC structures. In a more practical setting, Wang et al. [34] tackle the crucial problem of durability by examining how corrosion and fiber inclination interact to affect the pull-out response of steel fibers in cracked UHPC. Their results, which came from tests that mimicked exposure to environments high in chloride, show how susceptible steel fibers are to corrosion-induced deterioration, with the degree of damage varying according to both fiber shape and inclination angle. This emphasizes the necessity of suitable corrosion prevention techniques for UHPC constructions subjected to harsh environmental circumstances. The impact of fiber orientation and distribution on the pull-out behavior of specialized fiber types—more especially, arc-shaped and hooked-end fibers placed in a SIFCON matrix—is investigated by Li et al. [35]. They uncover intricate relationships that control the pull-out response by methodically altering the fiber spacing and inclination angles. Their research highlights how crucial it is to optimize the mechanical performance of fiber-reinforced composites by taking into account both the spatial arrangement of the fibers and their individual features.

In contrast to the general emphasis on skewed fiber geometries, Lee et al. [36] present a somewhat counterintuitive finding that straight steel fibers are likely to be more effective at enhancing the tensile strength of UHPC than hooked-end fibers, despite being less bond-intensive. This runs contrary to general expectation and demonstrates the possible relevance of other parameters, including fiber dispersion and efficiency of crack bridging, to the overall tensile behavior of UHPC. Complementing the potential of non-traditional fiber shapes, Kim et al. [36] explore the benefits of curved fibers in enhancing the tensile capacity of UHPC. Their results indicate that the enhanced mechanical anchoring offered by curved fibers can lead to greater tensile strength and ductility than straight fibers, opening up a promising avenue for the optimal utilization of fiber-reinforced concrete. Cao et al. [37], in a more theoretical paper, employ analytical modeling to study the effect of inclination angle on the pull-out mechanism of hooked-end fibers. Their model is able to predict an optimum inclination angle for optimal pull-out resistance, beyond which fiber fracture becomes the dominant mode of failure. This theoretical model is helpful in explaining the underlying mechanisms of fiber pull-out and can assist in the design of more efficient fiber reinforcement schemes. Experimental verification of the theoretical findings is provided by Lee et al. [38], who examine the effect of inclination on bond properties by means of direct pull-out testing. They demonstrate that maximum pull-out load is significantly increased when the angle of inclination is between 20° and 50°, as anticipated by the potential of an optimal inclination range for highest pull-out resistance. Further substantiating the above fact, Kim et al. [39] demonstrate that a 45° angle of inclination always produces a greater bond strength than 0° in the case of straight and curved fibers both.

Despite the considerable advantages of UHPC, the challenges related to its brittle failure behavior and the comprehensive understanding of the fiber-matrix interaction mechanism, particularly in the presence of nanomaterials, necessitate further rigorous investigation. Previous research has primarily focused on straight fibers or inclined fibers without considering the combined effect of CNTs and inclination angle on the pull-out response. Therefore, a comprehensive understanding of how these parameters simultaneously influence the adhesion mechanisms, strength, and ductility of CNT-reinforced UHPC composites is of paramount importance.

Therefore, this work aims to provide a more holistic perspective on the complex interactions between fibers, matrix, and nanomaterials by both experimentally characterizing and numerically simulating the pull-out response of inclined hooked-end steel fibers from a CNT-reinforced UHPC matrix. The key innovation of this research lies in the simultaneous examination of the influence of fiber inclination angle and CNTs content on the pull-out behavior, combined with the development of an improved finite element model utilizing cohesive zone theory (CZM). This model is calibrated and validated using direct tensile, compression, and inclined pull-out tests, enabling accurate prediction of the fiber-matrix interaction behavior in these advanced composites. The insights gained from this study can lead to the development of UHPC with optimized mechanical performance and provide more effective solutions for the design of resilient and durable structures.

2. Experimental tests

2.1. Materials and mix proportions

To achieve ultra-high compressive strength concrete (exceeding 150 MPa) in accordance with the recommendations of the American Concrete Institute (ACI) Committee 239, fine-grained materials were utilized in the production of the UHPC [40]. Type I Portland cement and silica fume were employed as the cementitious materials, and their chemical composition and physical properties are presented in Table 1. Silica sand and silica flour were also used as fine aggregate and filler, respectively, in the mixture. The particle size of the silica sand ranged from 0.25 to 0.4 mm, while the particle size of the silica flour was approximately 10 microns, consisting of 98 % silicon dioxide (SiO_2).

To examine the effect of nanomaterials on the mechanical properties of UHPC, CNTs were combined into the mixture at varying weight percentages relative to cement: 0 %, 0.1 %, 0.2 %, 0.4 %, and 0.6 %. The CNTs were supplied by Jiangsu Tiannai Technology Co., Ltd., Zhenjiang, China. To achieve a uniform dispersion of the CNTs within the concrete matrix, the CNTs were initially subjected to ultrasonic agitation in distilled water, along with a suitable dispersant. Fig. 1 presents a scanning electron microscope (SEM) image and a photograph of the CNT

Table 1
Physical properties and chemical composition of cementitious materials.

Component	Silica fume	Cement
CaO	0.39	62.13
SiO2	98.0	20.35
MgO	0.12	5.82
Al2O3	0.26	6.2
Fe2O3	0.14	3.15
SO3	-	2.35
Density (kg/m^3)	2180	3060
Specific surface area (cm^2/g)	3550	250,000

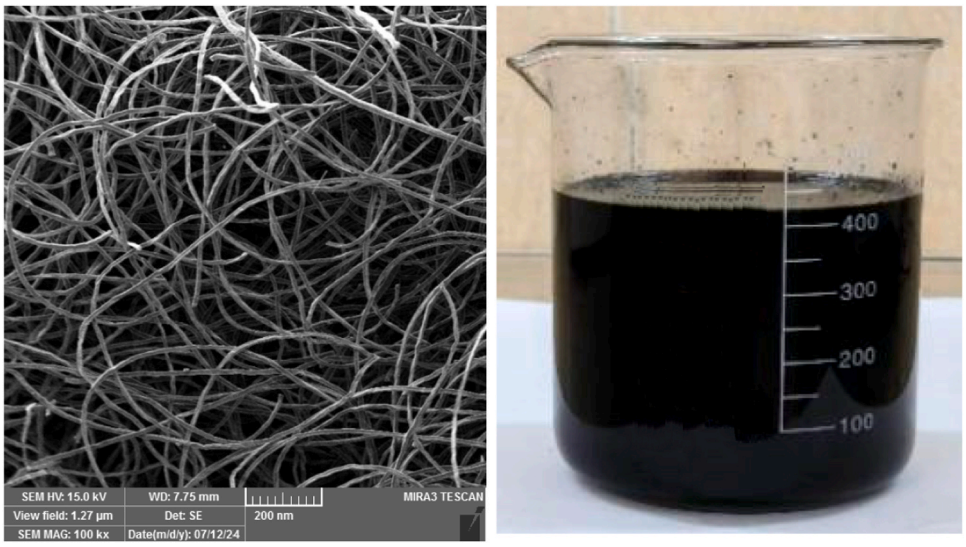

Fig. 1. SEM image and slurry mixture containing carbon nanotubes.

slurry. This process facilitates the effective dispersion of the CNTs within the cementitious mixture and prevents their agglomeration. Following preparation of the CNT-containing solution, this solution was added to the dry mixture of cement, silica fume, aggregates, and superplasticizer.

To ensure the workability and self-compacting properties of the concrete, a water-to-cementitious materials ratio of 0.2 was adopted. A polycarboxylate-based superplasticizer (SP) with a density of 1.16 g/cm^3 was also added to the mixture as a high-range water-reducing admixture. The detailed mix proportions for the UHPC are provided in Table 2. Due to the high superplasticizer dosage, a self-compacting UHPC with a flowability of approximately 250 mm, in accordance with ASTM C1437, was produced.

The steel fibers used in the pull-out tests were hooked-end steel fibers. The geometry of these fibers is shown in Fig. 2, and their mechanical properties are presented in Table 3. The hooked-end steel fibers selected for this study have a diameter of 0.7 mm and length of 50 mm, with tensile strength around 2100 MPa, representing typical industrial fibers widely used in concrete reinforcement [41–43]. Their relatively large size and hook geometry provide effective mechanical anchorage, critical for studying the pull-out versus rupture behavior. The embedded length was chosen to balance between enabling fiber pull-out and inducing fiber rupture, depending on the bond strength. Experimental results demonstrated that under high bond strength conditions (e.g., increased CNT content and fiber inclination), fibers ruptured before pull-out, confirming the appropriateness of the fiber selection and embedded length for investigating fiber-matrix interaction mechanisms in this study.

2.2. Specimen preparation

To determine the mechanical properties of the carbon nanotube-reinforced UHPC, compressive and tensile strength tests were performed. Compressive strength test specimens were prepared as cubes with dimensions of 50x50x50 mm^3, in accordance with ASTM C109. For

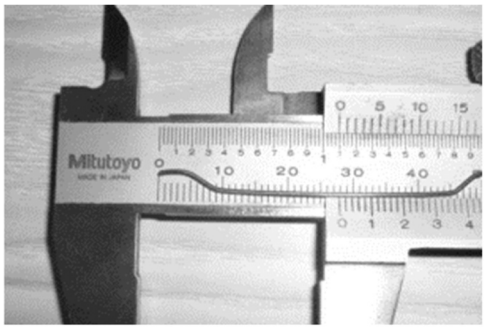

Fig. 2. Geometry of hooked-end steel fibers.

the direct tensile test, dog-bone specimens were fabricated in accordance with ASTM C307 to promote a more uniform stress distribution in the critical section. Fig. 3 shows the cubic specimens for the compressive strength test and dog-bone specimens for direct tensile test.

The concrete constituents were mixed according to the proportions presented in Table 2 and cast into standard molds. To reduce entrapped air voids and improve compaction, the molds were subjected to mechanical vibration. After casting, the specimens were cured at ambient temperature for 24 h and then immersed in saturated limewater for 28 days to achieve their ultimate strength.

To investigate the fiber pull-out behavior, cylindrical specimens containing hooked-end steel fibers oriented at various angles (0°, 30°, 45°, and 60°) relative to the concrete surface were fabricated. As shown in Fig. 4, the pull-out specimen molds were cylindrical with dimensions of 50 mm× 50 mm. Fibers with a specified embedded length and angle were carefully positioned at the center of the cylindrical mold, which was subsequently filled with concrete and vibrated on a vibrating table. The process of embedding the fibers within the concrete was performed with precision to ensure repeatability of the results. Lastly, to investigate

Table 2
Mix proportions of carbon nanotube-reinforced ultra-high performance concrete.

Specimen	Cement	CNT	Silica fume	Fine aggregates	Silica powder	Superplasticizer	Water/cement
UHPC (Ref.)	1.000	0.000	0.25	1.1	0.35	0.04	0.2
CNT0.1	0.999	0.001	0.25	1.1	0.35	0.04	0.2
CNT0.2	0.998	0.002	0.25	1.1	0.35	0.04	0.2
CNT0.4	0.996	0.004	0.25	1.1	0.35	0.04	0.2
CNT0.6	0.994	0.006	0.25	1.1	0.35	0.04	0.2

Table 3
Geometric and mechanical properties of hooked-end steel fibers.

Type	Diameter	Length	Density	Yield Strength	Tensile strength	Elongation at rupture	Elastic modulus
Hooke shape	0.7 mm	50 mm	7800 kg/m^3	800 MPa	2100 MPa	6.3 %	208 GPa

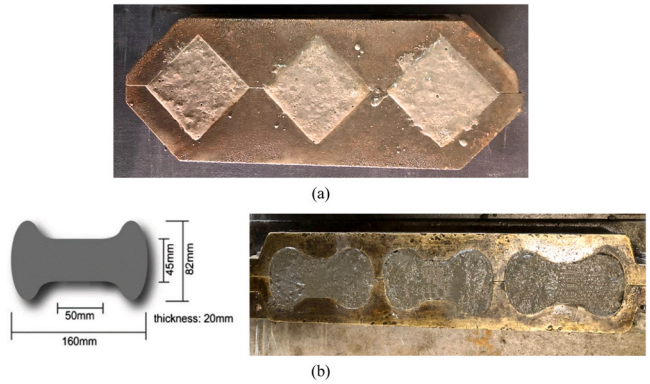

Fig. 3. (a) Cubic specimens for compressive strength test and (b) dog-bone specimens for direct tensile test.

the bond between the fibers and the concrete matrix, fiber pull-out experiments were performed on the specimens.

2.3. Experimental procedures

In this study, specimens with different concentrations of carbon nanotubes underwent direct tensile and uniaxial compressive testing to ascertain the mechanical characteristics, such as the stress-strain curves, needed for the ABAQUS program. A universal testing equipment with a tensile capacity of 5 kN was used to test the dog-bone specimens in order to determine the tensile stress-strain curve. After securing the dog-bone specimens with a steel grip, a statically applied uniaxial tensile force was applied at a rate of 0.5 mm/min. Linear variable displacement transformers were used to measure and record the specimen's elongation, while a load cell monitored the force under displacement-controlled loading. To extract the compressive stress-strain curve, the specimens were exposed to uniaxial compressive loading at a rate of 2 mm/min via the same universal testing machine. Fig. 5 shows the universal testing machine used. The pull-out experiments were also accomplished under displacement control at a rate of 0.2 mm/min. To apply the tensile force, the free end of the fiber was placed within the machine's gripping jaws. To minimize errors in slip measurements due to fiber elongation, the distance between the jaws was designed to be as close as possible to the specimen surface. For each test, three identical specimens were fabricated, and all specimens were loaded to failure.

3. Finite element simulation

The finite element method, by enabling precise analysis and simulation of complex structural and material behaviors, serves as a powerful tool for solving engineering and scientific problems and plays a crucial role in optimizing designs and predicting system performance [44–46]. Using ABAQUS software, nonlinear FEM was carried out to model the pull-out performance of inclined hooked-end steel fibers from carbon nanotube-reinforced UHPC. The steel fiber and CNT-reinforced UHPC components were modeled independently for this FEM, as seen in Fig. 6. A mesh sensitivity analysis was carried out to identify the ideal element

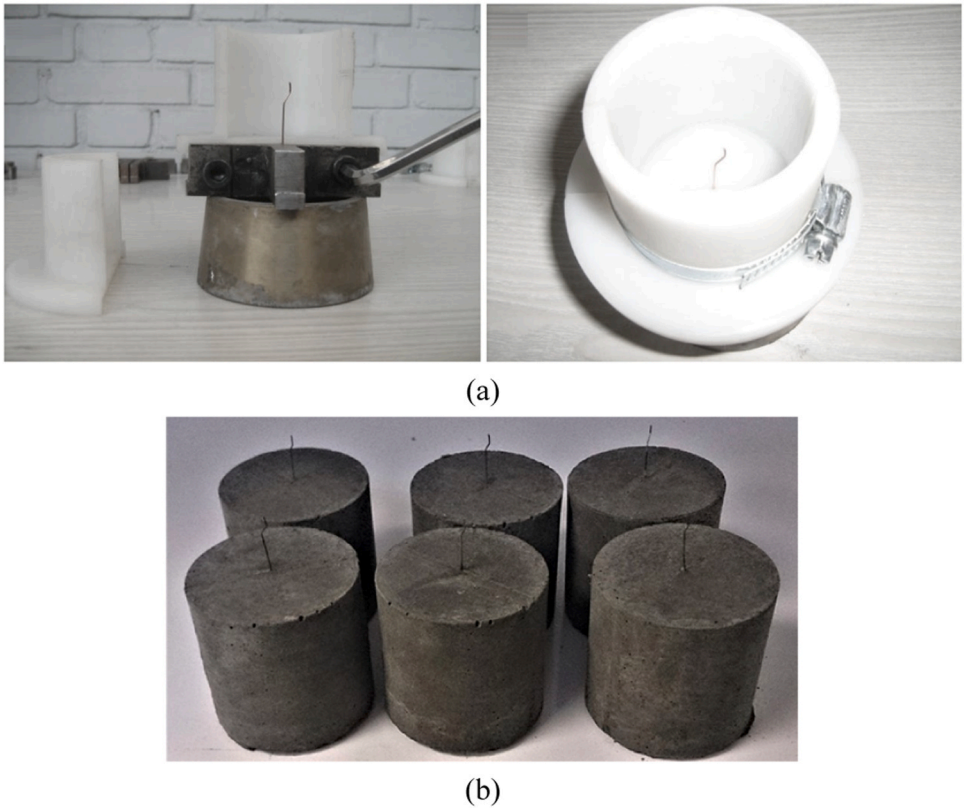

Fig. 4. (a) Mold for fiber pull-out specimens and (b) fiber pull-out test specimens.

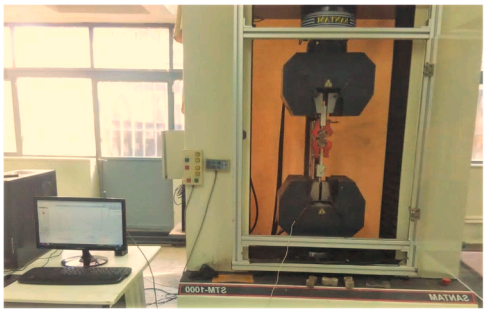

Fig. 5. Universal testing machine used for direct tensile, direct compression, and fiber pull-out tests.

size that strikes a compromise between computational cost and solution accuracy in order to guarantee the precision and dependability of the finite element results. This analysis involved systematically refining the mesh and monitoring key output parameters, such as peak pull-out force and interfacial stress, until further mesh refinement yielded negligible changes in these results. The concrete and steel fiber were meshed using 20-node quadratic brick elements (C3D20R), and to prevent shear locking phenomena, reduced-integration elements available in ABAQUS were employed. The adhesion at the steel fiber-concrete interface was then modeled using zero-thickness cohesive components. The bilinear cohesive zone model (CZM) served as the foundation for the cohesive components. The most popular and efficient model for describing the contact between fibers and the concrete matrix is the bilinear CZM. Fig. 7 illustrates the constitutive curve for this model in the normal direction.

In the bilinear CZM, the parameter $\tau_{\max}$ represents the critical shear strength, defined as the extreme bond load that the interface can withstand prior to the onset of separation. The parameter $\delta_{\max}$ denotes the critical displacement at point of failure, expressive the maximum slip distance over which the interfacial bond strength can be transmitted. When the displacement ($\delta > \delta_{\max}$), complete interfacial separation and detachment of the elements on either side occur. The area under the $\tau \sim \delta$ curve represents the interfacial fracture energy, G_C. The parameter K represents the tangent stiffness prior to the onset of mechanical property degradation. Interfacial fracture energy (G_C), bond strength (τ), and slip (δ) are considered three fundamental constants in the CZM, and their relationship can be stated by the following equation:

$$G_c = \frac{1}{2}\tau_{\max}\delta_{\max} \tag{1}$$

An assessment framework from damage initiation to damage evolution is present in the bilinear cohesive element model. To ascertain when damage starts and, as a result, when stiffness degradation starts, the damage initiation criterion is applied. The criterion for the first

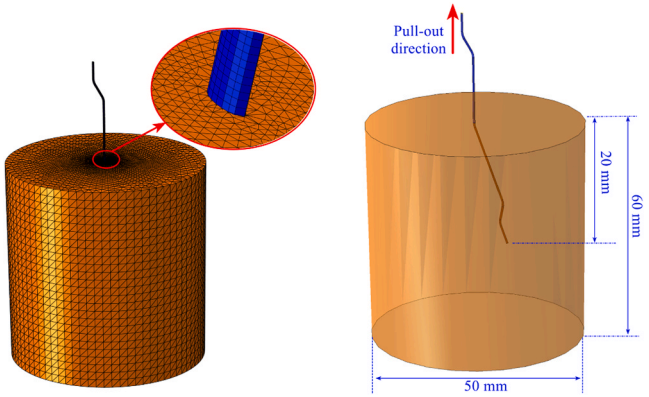

Fig. 6. Finite element model of fiber pull-out and meshed model.

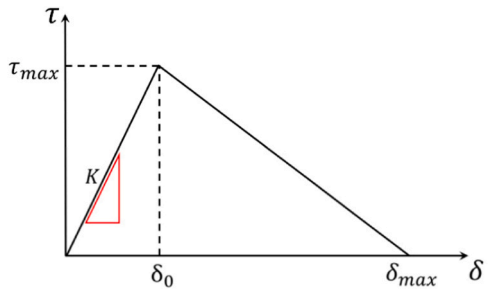

Fig. 7. Bilinear cohesive zone model.

damage beginning in this investigation is the highest nominal stress. The condition for initial damage occurrence is expressed as follows:

$$\max\left\{\frac{<\tau_n>}{\tau_n^0}, \frac{<\tau_t>}{\tau_t^0}\right\} = 0 \tag{2}$$

In this equation, τ_n and τ_t denote the effective stress in the normal and tangential directions relative to the crack plane, respectively; and τ_n^0 and τ_t^0 represent the maximum stresses that the element can withstand in the normal and tangential directions relative to crack plane, respectively.

The process of damage evolution is monitored once initial damage has been caused. Stiffness reduction is a defining characteristic of mechanical property deterioration, while the CZM damage evolution criterion establishes the connection between separation displacement and traction force. The following is an expression for damage evolution:

$$D = \begin{cases} 0 & \delta \le \delta_0 \\ \dfrac{\delta_{\max}(\delta - \delta_0)}{\delta(\delta_{\max} - \delta_0)} & \delta > \delta_0 \end{cases} \tag{3}$$

Stiffness degradation is characterized by the parameter D, which ranges from 0 to 1. A value of $D = 0$ indicates that no damage has happened, whereas $D = 1$ signifies complete failure. After damage occurrence, the element stiffness during degradation is denoted by K_0. The stiffness of element is reduced due to damage phenomena according to following relation

$$K_0 = (1 - D)K \tag{4}$$

The binding strength and fracture energy values of the cohesive elements at the boundary layer are frequently unknown in FEM calculations. An experimental computational approach is used to ascertain the cohesive elements parameters. The ideal parameters are found by comparing the load-slip curves produced by the numerical simulations with experimental findings after varying the bond force and fracture energy values.

The mechanical properties for the five concrete mixes, corresponding to the mix proportions in Table 2, were obtained from experimental testing. The concrete was modeled using the Concrete Damaged Plasticity (CDP) model, and the tensile and compressive stress-strain curves for each mix were derived from the corresponding experimental tests. The CDP model also requires five key parameters. These five parameters include the ratio of biaxial to uniaxial compressive strength (K_c), the dilation angle, the viscosity parameter, and tensile and compressive hardening parameters. Their values were determined based on reputable references and prior studies [31] and are listed in Table 4. The parameters used in the CDP model (Table 4) were primarily adopted from established literature on UHPC with CNTs [31,47]. These parameters have been validated experimentally in previous studies and are known to effectively represent the nonlinear behavior of UHPC. Although specific CDP parameter values for CNT-reinforced UHPC are limited in the literature, the primary effect of CNT addition is reflected in changes to the tensile and compressive strength and fracture energy, which were updated based on our experimental results. Other plasticity parameters,

Table 4
Values of the five key parameters in the CDP model.

Parameter	Symbol	Value Range
Biaxial to uniaxial stress ratio	K_c	0.667
Dilation angle	ψ	35°
Viscosity parameter	μ	0.001
Tensile hardening ratio	f_t/f_c	0.06
Compressive hardening ratio	f_{b0}/f_{c0}	1.16

such as dilation angle, viscosity, and hardening ratios, were assumed to remain constant, consistent with common practice and due to the lack of conclusive data indicating significant changes. The CDP model has been widely applied and validated for UHPC by various researchers, and its use in this study provides a reliable framework for simulating the material behavior of CNT-reinforced UHPC.

The steel fibers were modeled as a strain-hardening, elastic-plastic substance. The stress-strain behavior of steel fibers is quite similar to that of conventional reinforcing bars. In this study, the bilinear kinematic hardening plasticity model is employed to simulate the structural behavior of steel fibers [48]. During the hardening phase, the slope of the stress-strain curve is assumed to be 1 % of the initial elastic modulus, i.e., $E = 0.01E_0$. According to Table 3, the initial elastic modulus of the steel fiber is 208 GPa, with a Poisson's ratio of 0.27, elongation at rupture of 6.3 %, and a tensile strength of 2100 MPa. The failure of steel fibers was simulated using the shear failure criterion available in ABAQUS, which is based on a critical strain at failure, effectively capturing fiber fracture under tensile loading. The analysis was performed quasi-statically to ensure the stability of the results. The fibers were embedded in the concrete at one end, and the other end was subjected to a uniaxial tensile load. To prevent undesirable movement, appropriate boundary conditions were applied to the simulated specimens.

4. Results

This section presents the results of the finite element analyses and experimental tests conducted to investigate the influence of various parameters – including embedment angle and CNT content – on the fiber pull-out characteristics. First, the effect of CNT content on the mechanical properties of the UHPC is discussed. Next, the CZM parameters corresponding to varying CNT concentrations are determined, and the accuracy of the finite element results is evaluated. Finally, the effects of various parameters on the pull-out characteristics of inclined steel fibers are examined.

4.1. Effect of CNTs on mechanical properties

Fig. 8(a) shows the tensile stress-strain curves for the reference sample and the samples reinforced with 0.1 %, 0.2 %, 0.4 %, and 0.6 % CNTs by weight. The results show that the adding of CNTs to UHPC has a significant influence on the tensile strength. As shown in Fig. 8(b), the tensile strength of the reference sample was 7.78 MPa, which increased with increasing CNT content up to 0.4 %, reaching 9.18 MPa. This corresponds to a 17.9 % improvement compared to the reference sample. This increase in strength can be attributed to improved adhesion between the CNTs and the concrete matrix, uniform stress distribution, and reduced crack formation at the nanoscale. However, in the 0.6 % CNT sample, the tensile strength decreased to 8.04 MPa, likely due to CNT agglomeration and reduced concrete homogeneity at higher percentages. These results suggest that 0.4 % CNTs is the optimum content for improving the tensile strength of UHPC. Higher contents have a negative impact on strength due to the formation of weak zones resulting from non-uniform distribution and an increased demand for superplasticizers. Furthermore, upon application of stress to the samples, the stress rapidly decreases after reaching the tensile strength, indicating brittle failure characteristics. This behavior suggests that, despite the improved tensile strength, the fracture toughness of the CNT-reinforced concrete may still be a challenge and requires further investigation regarding surface modification of the nanotubes and its effects on the failure mechanism. It should be noted that Fig. 8 illustrates the tensile behavior of UHPC without steel fibers, focusing on the matrix reinforced only with varying CNT contents. The sudden drop in tensile stress corresponds to the brittle fracture of the UHPC matrix. Fiber-related effects on tensile behavior are analyzed separately in the pull-out experiments.

Fig. 9 shows the compressive stress-strain curves and compressive strength of the reference sample and the samples reinforced with varying CNT contents. The specimens demonstrated strain hardening behavior. In the elastic stage, the compressive stress increases linearly with increasing compressive strain up to approximately 1.5×10^{-3}. In the strain-hardening stage, the sample reaches the ultimate compressive strength (σ_{pc}) during the process of transitioning from the initial cracking strain (ε_{fc}) to the ultimate compressive strain (ε_{pc}). Beyond this point, in the strain-softening stage, the stress decreases nonlinearly with increasing compressive strain. The peak compressive stress increases with increasing CNT content. The results presented in Fig. 8 indicate that the addition of CNTs to UHPC has a significant effect on compressive strength. The reference sample had a compressive strength of

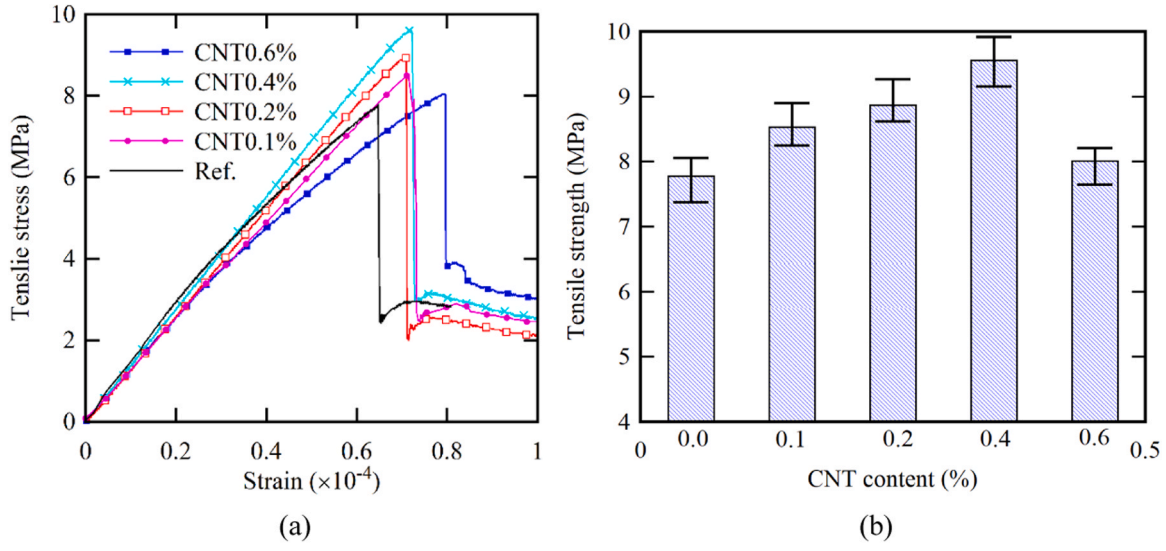

Fig. 8. (a) Tensile stress-strain curves and (b) tensile strength of the reference sample and samples reinforced with varying CNT contents.

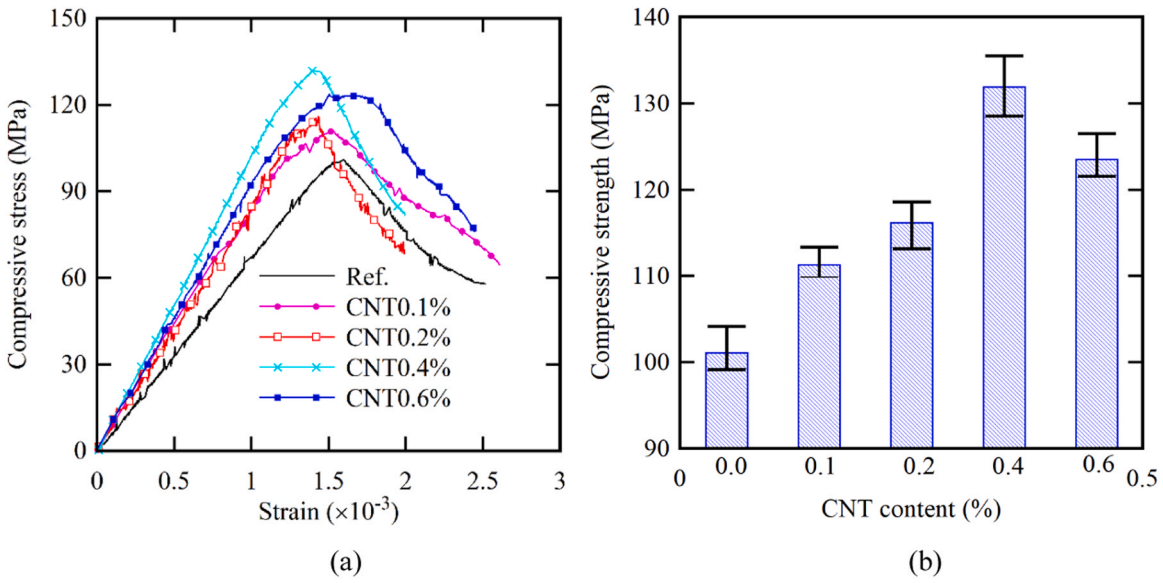

Fig. 9. (a) Compressive stress-strain curves and (b) compressive strength of the reference sample and samples reinforced with varying CNT contents.

101.09 MPa, which increased with the addition of CNTs up to 0.4 %, reaching a value of 131.91 MPa. This increase represents approximately a 30.6 % improvement compared to the reference sample, which can be attributed to the increased bonding between the cement matrix and nanotubes, improved stress transfer at the nanoscale, and a reduction in microscopic defects.

However, in the 0.6 % CNT sample, the compressive strength decreased to 123.76 MPa. This strength reduction may be due to excessive agglomeration of the nanotubes and a decrease in the uniformity of their distribution within the concrete matrix, leading to the

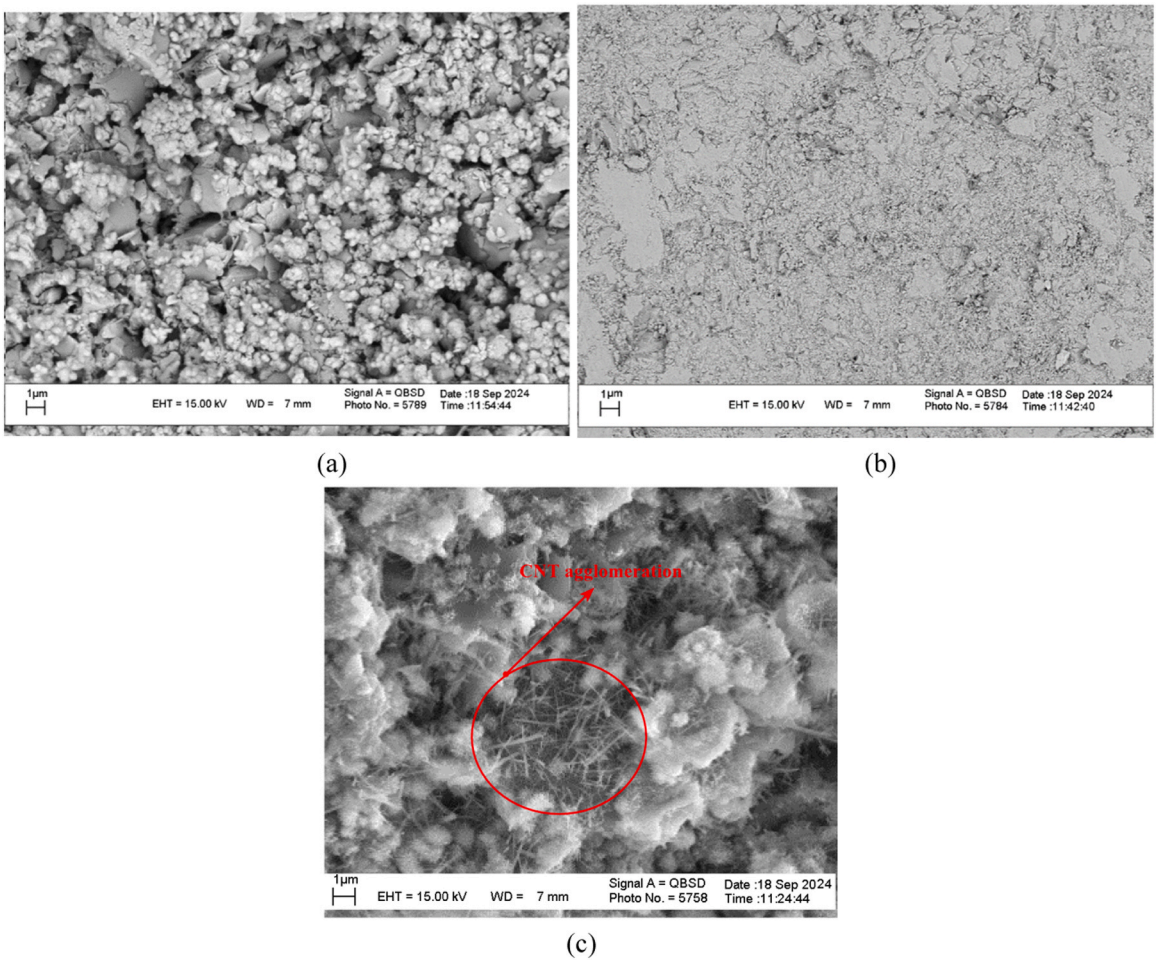

Fig. 10. SEM images of the fracture surface of (a) reference UHPC, (b) UHPC reinforced with 0.4 % CNT, and (c) UHPC reinforced with 0.6 % CNT.

formation of weak zones and the creation of localized stress concentrations. Also, the value of X, which represents the strain corresponding to the maximum stress, decreases with increasing CNT percentage up to 0.4 % and then increases again, indicating a decrease in the ductility of the samples at higher CNT percentages. These results indicate that 0.4 % CNTs is the optimum content for improving the compressive strength of UHPC, while higher percentages may have a negative impact on the mechanical behavior of the concrete. To demonstrate the consistency and reliability of the experimental results despite the limited number of specimens, Figs. 8(b) and 9(b) present the minimum and maximum tensile and compressive strengths, respectively, obtained for each CNT content. The data reveal that variations in mechanical properties among replicates remain within 5 %, confirming the reproducibility of the testing procedure and the homogeneity of the specimens.

Fig. 10 shows SEM images of the fracture surface of UHPC samples. Fig. 10(a) shows the fracture surface of the reference UHPC sample, which exhibits a relatively brittle fracture and a highly porous structure in the absence of carbon nanotubes. The porous microstructure observed is indicative of voids and microcracks formed during hydration and curing, which act as stress concentrators and weaken the overall matrix. The absence of CNTs results in limited crack-bridging mechanisms and lower energy absorption capacity, explaining the brittle behavior and lower tensile strength of the reference sample. In contrast, Fig. 10(b) shows the fracture surface of UHPC reinforced with 0.4 % CNTs. The SEM image reveals a markedly denser microstructure with a significant reduction in porosity and microcracking. The CNTs are well-dispersed within the matrix, forming effective nanobridges across microcracks. This bridging action delays crack propagation by transferring stress and enhancing load redistribution, thereby increasing toughness and ductility. The improved fiber-matrix adhesion is attributed to the high specific surface area and strong interfacial bonding of CNTs with the cementitious phases, which also contributes to increased mechanical strength and improved fracture energy. These effects collectively shift the failure mode from brittle to more quasi-ductile behavior, as confirmed by the more tortuous crack paths and rough fracture surfaces. Fig. 10(c) presents an additional SEM image highlighting the agglomeration of CNTs observed in the 0.6 % CNT sample. This image clearly demonstrates the formation of CNT clusters, confirming non-uniform dispersion at higher concentrations and supporting the observed decrease in mechanical performance.

4.2. Determination of CZM parameters and validation of FEM results

To accurately simulate the pull-out performance of hooked-end steel fibers from carbon nanotube-reinforced UHPC, the CZM was employed. Determination of the CZM parameters, including the ultimate bond strength (τ_{max}), fracture energy (G_c), initial stiffness (K), and displacement corresponding to the ultimate bond strength (δ_0), was performed using a trial-and-error approach [49–51] for each concrete mix. These values were adjusted such that the slip-pull-out curve from the finite element simulation results matched the experimental data. Table 5 presents the final determined values for each mix. It can be observed that as the CNT content increases, the values of ultimate bond strength and fracture energy increase, reaching their maximum values in the 0.4 % CNT mix. This increase indicates improved adhesion between the concrete matrix and the steel fibers, as well as an increased ability of the concrete to resist cracking. However, in the mix containing 0.6 % CNT, a slight decrease in some parameters is observed, which may be due to CNT agglomeration and a reduction in their uniform dispersion within the concrete matrix. The finite element model results, using these parameters, were compared with the experimental data, and acceptable agreement was observed, indicating the validity of the parameter calibration in the numerical simulation. The displacement at maximum bond strength (δ_0) is calculated from τ_{max} and K ($\delta_0=\tau_{max}/K$) and is included for completeness, rather than as an independent calibration parameter. The three primary CZM interface parameters were calibrated using a trial-and-error method to closely match the slip-pull-out curves obtained from experiments. Calibration was conducted primarily with pull-out tests on aligned fibers (0° inclination) for each CNT content, using the average results from three replicate tests to ensure reliability. The resulting calibrated parameters were then applied to simulate inclined fiber pull-out without modification, under the assumption that interface properties are independent of fiber orientation. This procedure ensures a consistent and robust numerical representation of the fiber-matrix interface.

Table 5
Final values of CZM parameters for different mix designs.

Mix. type	τ_{max} (MPa)	G_c (N/mm)	K (N/mm^3)	δ_0 (mm)
Ref. (CNT0.0)	3.5	0.12	7.78	0.45
CNT0.1	4.2	0.15	8.75	0.48
CNT0.2	4.8	0.18	9.60	0.50
CNT0.4	5.3	0.22	12.61	0.42
CNT0.6	4.9	0.20	9.81	0.50

4.3. Comparison between results of FEM and experimental tests

Fig. 11 presents a comparison between the uniaxial tensile and compressive stress-strain curves obtained from the finite element simulation and the corresponding experimental results shown in Figs. 8 and 9. The numerical model, based on the CDP framework with calibrated parameters, exhibits good agreement with the experiments for all CNT content levels. This confirms the validity of the model in accurately capturing the mechanical behavior of CNT-reinforced UHPC. Since the exact experimentally measured mechanical properties were directly used as input material data in ABAQUS, the good agreement between numerical and experimental results was expected, confirming the validity of the calibrated CDP model for CNT-reinforced UHPC

Fig. 12 presents a comparison of the slip-pull-out force curves for straight hooked-end steel fibers from UHPC, obtained from experimental results and the FEM. In this simulation, the coefficients of the CZM were applied according to the values presented in Table 5. As can be observed, the pull-out force values obtained from the FEM are slightly higher compared to the experimental tests. A detailed re-analysis of Fig. 12 reveals that the deviation between the finite element model predictions and the experimental pull-out forces lies within a tighter range of 3–7 %. This improved agreement demonstrates the high accuracy of the numerical model and validates its effectiveness in simulating the fiber pull-out behavior in CNT-reinforced UHPC. The cause of this discrepancy may be due to the method of determining the CZM parameters, numerical assumptions related to the fiber-matrix contact model, as well as differences in the actual loading conditions compared to the idealized conditions in the numerical model. Overall, the results indicate that the finite element model has a high capability in predicting the pull-out behavior of fibers, but to achieve greater accuracy, some experimental parameters can be entered into the model in an optimized manner. Qualitatively, the overall trend of the pull-out force-slip curves in the numerical model and experimental test is similar, indicating that the finite element model, using appropriate CZM coefficients, has been able to accurately describe the overall behavior of the system. However, the difference in the obtained values indicates that some influencing parameters, such as the interaction between the fiber and the concrete matrix or the method of dispersion of the carbon nanotubes, have not been fully considered in the modeling. The finite element model tends to slightly overestimate pull-out forces due to idealized assumptions such as perfect bonding, omission of microcracking and material defects (e.g., air voids), and simplified boundary conditions. These factors reduce bond strength in real specimens, which is not fully captured in the numerical model.

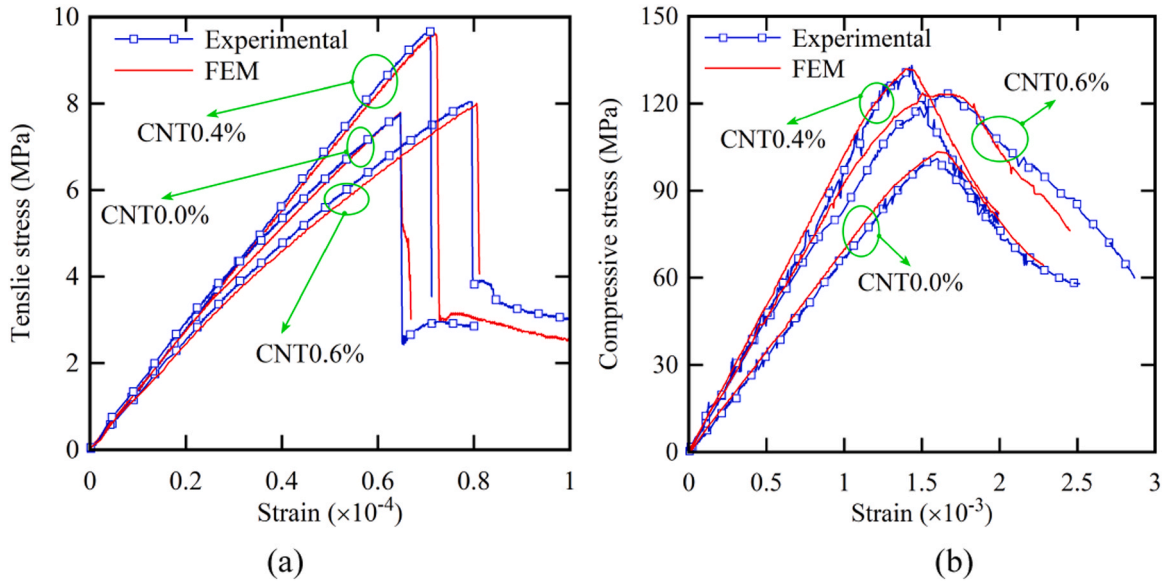

Fig. 11. Comparison of uniaxial tensile (a) and compressive (b) stress-strain curves obtained from finite element simulations and experimental tests for UHPC samples with varying carbon nanotube contents.

4.4. Finite element analysis results

The results obtained from the FEM of fiber pull-out are presented as force-slip diagrams for different weight percentages of carbon nanotubes, including 0 %, 0.1 %, 0.2 %, 0.4 %, and 0.6 %, and with fiber inclination angles of 0°, 15°, 30°, 45°, and 60° relative to the perpendicular axis. The results pertaining to the maximum pull-out load, the slip corresponding to the maximum force, the pull-out energy, and the ratio of the maximum stress obtained in the fiber to its ultimate tensile strength (σ_{max}/f_u) – representing the effectiveness of the fiber – were calculated and presented for each sample, along with their average values in each case.

The resistance of the fibers to being pulled out of the matrix results from two factors: friction and mechanical anchorage. Friction depends on the quality of the contact surface between the fiber and the matrix, as well as the properties of the materials in the contact area. This is greatly reduced as slip increases. Mechanical anchorage results from the geometry of the fibers and how they are deformed. This factor is activated after complete separation of the fiber from the matrix and after a small amount of slip, and it maintains its resistance, depending on the quality of the anchorage, until significant deformation. Fig. 13 shows the force-slip curve for a sample containing 0.1 % carbon nanotubes with an inclination angle of 30°. As can be seen, the behavior of the pull-out of hooked fibers is described in several stages. Stage 1 is the elastic stage or the beginning of the separation of the fiber from the matrix. In this stage, the elastic shear stress at the contact surface of the fiber and matrix is higher than the cohesion resistance, and when the pull-out force reaches P_{cr} and the amount of slip reaches Δ_{cr}, the separation of the fiber from the concrete matrix begins. Stage 2 is the partial separation (between Δ_{cr} and Δ_{max}), where the stresses in this stage are a combination of adhesion and frictional stresses, and the sum of these stresses is greater than the force related to the pull-out. When P_{cr} reaches P_{max}, the pull-out force of the fiber overcomes the sum of the internal stresses of the interface between the fiber and the matrix, and the fiber completely separates from the matrix, after which a sudden drop occurs in the diagram. Stage 3 is the effect of mechanical anchorage and the creation of plastic hinges (between Δ_{max} and Δ_0), in which the fiber begins to deform and move within the matrix. The deformation applied to the fiber creates a plastic hinge that will be displaced during pull-out. At the beginning of this stage, two plastic hinges are created, and after a certain amount of pull-out, one hinge is removed, leaving only one hinge. The creation of plastic hinges increases the fiber's resistance to being pulled out. Stage 4 is frictional pull-out. After the adhesion stress is lost at the surface of the fiber and the matrix, the pull-out resistance is completely supplied by friction. After the plastic hinges are removed and the slip increases in this stage, the pull-out resistance of the fiber from the concrete matrix gradually decreases, and the fiber will be pulled out of the matrix.

Fig. 14 shows the deformation of the fiber and the different stages of pull-out for two forces, P_{max} and P_0. As can be seen, for P_{max}, the mechanical engagement of the hook section with the concrete is eliminated, and at P_0, the fibers completely lose their mechanical engagement due to the destruction of the concrete in the areas around the curved sections.

Fig. 15 shows the force-slip curves for UHPC samples containing 0 %, 0.1 %, 0.2 %, 0.4 %, and 0.6 % CNTs, with inclination angles of 0°, 15°, 30°, 45°, and 60° relative to the perpendicular axis. As can be seen, in general, with increasing CNT content, the fiber pull-out force increases, which is a result of strengthening the adhesion of the fibers to the concrete, as well as increasing the contribution of mechanical engagement due to the greater strength of the concrete. From a physical perspective, increasing CNTs content improves the mechanical properties of UHPC. Due to their high specific surface area and strong interaction with the cement matrix, carbon nanotubes increase the adhesion between the steel fibers and the concrete, thereby strengthening the friction mechanism and the mechanical engagement of the fibers in the matrix. This strengthening ultimately leads to an increase in the fiber pull-out force. In addition, the greater strength of the CNT-reinforced concrete limits the growth of microcracks around the fibers, thereby improving the resistance to pull-out.

From a mechanical perspective, the influence of fiber inclination angle on the pull-out force is due to changes in shear and tensile components of the forces transmitted along the fiber. At small inclination angles (0° to 45°), increasing the angle leads to an increase in the pull-out force because the force component acting in the direction of fiber pull-out increases. However, for angles greater than 45°, the influence of the shear mechanism on the pull-out resistance increases, and the amount of force required to pull out the fiber decreases. At an inclination angle of 60°, due to the reduction in the effective area of fiber engagement with the concrete matrix and the increase in stress concentration at the contact point, the pull-out force is even less than the value for fibers perpendicular to the concrete surface (0° inclination angle). This behavior indicates that there is an optimum angle to improve the fiber-concrete engagement mechanism, which was observed in this study to

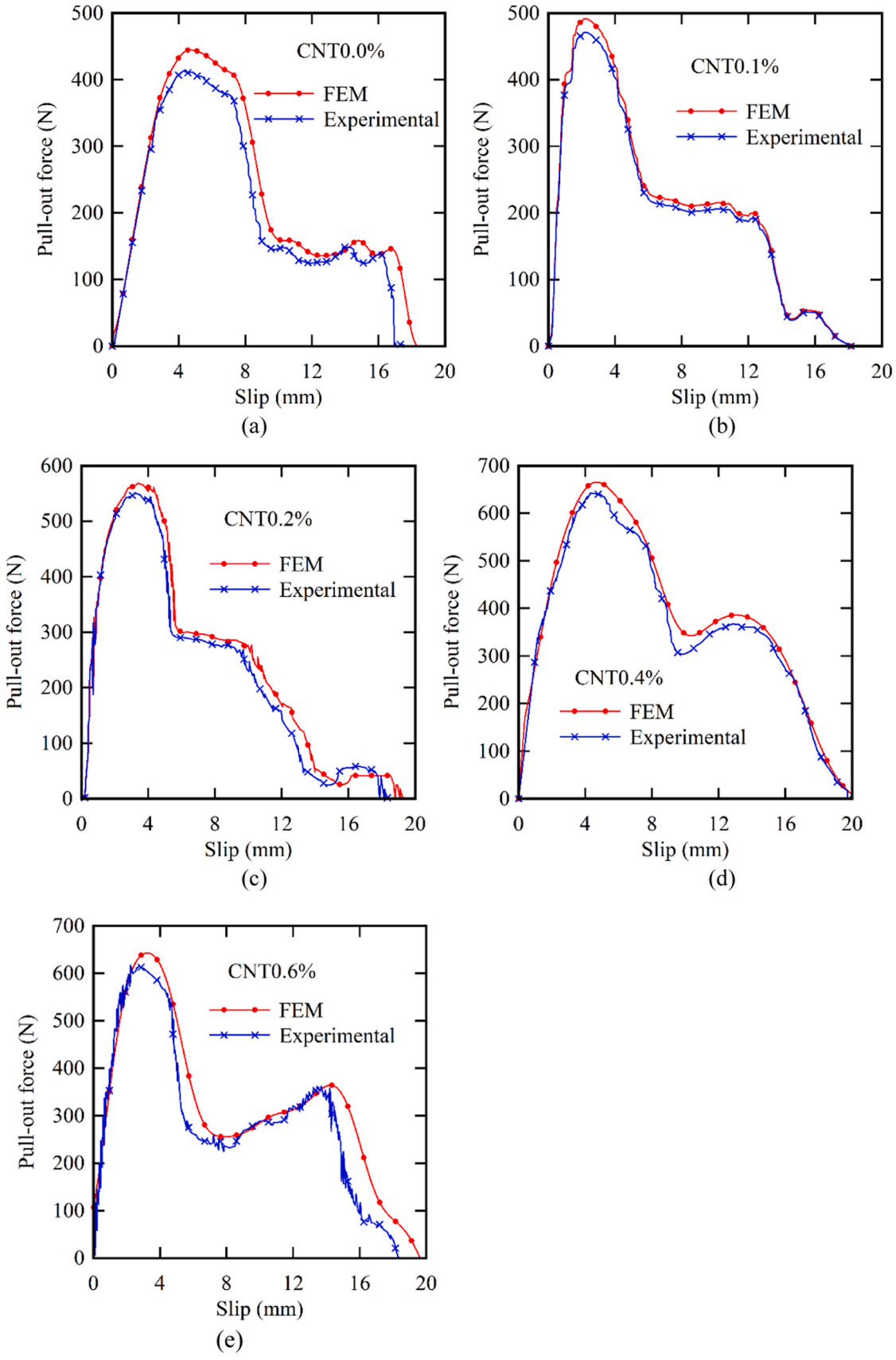

Fig. 12. Comparison of slip-pull-out force curves for straight hooked-end steel fibers from UHPC.

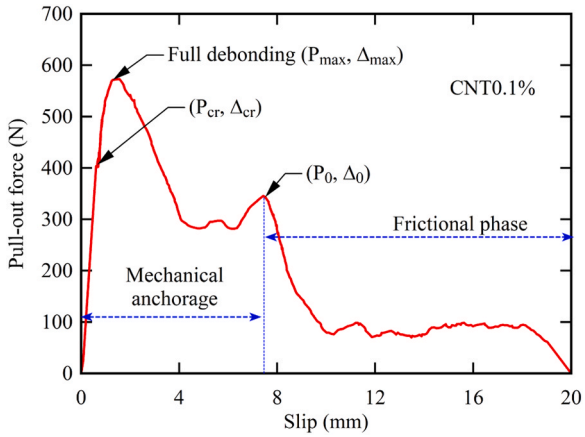

Fig. 13. Force-slip curve for sample containing 0.1 % CNTs with an inclination angle of 30°.

be in the range of 45°.

The abrupt drops and sudden termination of some force-slip curves in Fig. 15 correspond to fiber rupture during pull-out, primarily observed in samples with 0.4 % CNT content and fiber inclination angle of 30° and above. The increased bond strength under these conditions causes the tensile stress in the fiber to exceed its ultimate strength, leading to sudden breakage. The fiber failure mechanisms for the tested samples are summarized in Table 6, distinguishing between pull-out and rupture modes depending on CNT content and inclination angle. Experimental inspection confirmed fiber failure near the hook region, where stress concentrations are highest. The finite element model, using a shear failure criterion based on critical strain, effectively predicts these rupture events and their locations. This correlation validates the model's capability to capture complex fiber failure mechanisms alongside pull-out behavior.

For fiber pull-out at inclination angles greater than 30°, the fibers were not pulled out from the center of the specimen. Instead, it was observed that the fibers straightened along the loading direction, causing matrix crushing up to a point at a distance from the specimen center before pull-out. The same phenomenon was observed in the case of fiber rupture. Fig. 16 provides a comparison between the final deformed shape of the fibers and their failure mechanism in the experimental tests and finite element simulations. In the force-slip diagrams of steel fiber pull-out from the matrix, it was observed that, at inclination angles higher than 30°, the CNT content is reduced due to localized crushing of the matrix and spalling at the fiber exit point, leading to a decrease in the maximum force value. Because of matrix spalling and the snubbing effect, the damage process of inclined fibers with end deformation is complicated. The following are included in this damage: The fiber end deformation scratches the matrix tunnel; (1) the side of the fiber farther from the fiber penetration plane debonds earlier than the other side, and the clearance between the fiber and the matrix gradually increases; (2) the matrix near the fiber exit point gradually cracks, fractures, and spalls.

Fig. 17 shows the deformation of the fibers after being pulled out of the cement matrix for concrete containing 0.2 % CNTs with a 45° fiber inclination. As can be seen, the fibers are pulled out of the matrix along with plastic deformation and the formation of plastic hinges, and the predicted deformation pattern for the fibers has acceptable agreement with the experimental results. Both numerical and experimental images in Fig. 16 demonstrate that the hooked-end steel fibers are pulled out from the UHPC matrix without rupture. The fibers exhibit plastic deformation, such as bending or straightening of the hook, rather than fracture. This observation confirms that fiber failure did not occur and the changes in fiber shape result solely from plastic deformation during pull-out.

Table 6 presents an analysis of the impact of fiber inclination angle relative to the loading direction and the CNT content of the fibers on the pull-out response. The pull-out response consists of the pull-out force, the slip corresponding to the maximum force, the pull-out energy, the fiber utilization ratio, and the extent of matrix spalling in each scenario. According to the results in Table 6, inclined hooked-end steel fibers exhibit a higher bond strength against pull-out than fibers oriented at 0° due to the additional mechanical interlock resulting from the hook shape and the "snubbing" effect. In addition to friction and the existing chemical bond on the fiber surface, this mechanical interlock increases the resistance against pull-out, thus improving the mechanical performance of the UHPC. This mechanism results from stress concentration and localized crushing of the matrix in the region of the fiber tunnel exit, as shown in Fig. 18. In this region, contact pressures between the fiber and matrix are high, leading to increased frictional stresses. As a result, the combination of the bond and increased frictional stresses creates a higher bond strength compared to aligned fibers. With an increase in the angle from 0 to 15 degrees, the pull-out force has increased in all samples, indicating an improvement in the mechanical engagement of the fibers with the concrete matrix at this angle. The greatest increase was observed in the CNT-0.4 % sample, with a 17.63 % increase in the pull-out force, while the smallest increase was associated with CNT-0.6 % at 3.06 %, which may indicate a reduced effect of carbon nanotubes at high quantities. In samples containing CNT, the general trend shows that adding CNT improves adhesion and increases the pull-out force. This effect is less apparent in samples with larger quantities of CNTs. The samples containing CNT also showed an increase of effect on adhesion

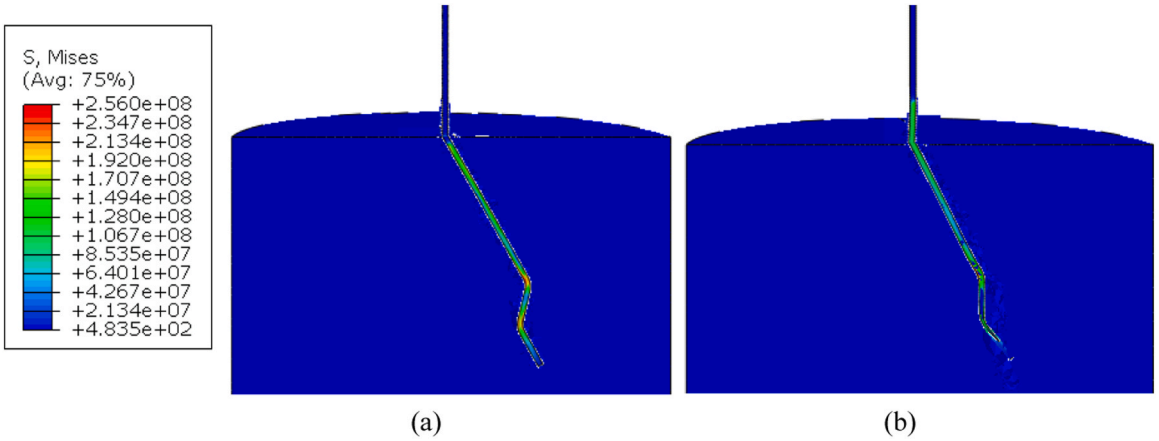

Fig. 14. Stress distribution and deformation of the fiber in a sample containing 0.1 % CNTs with an inclination angle of 30° for different values of applied force, (a) P_{max}= 592 N and (b) P_0= 382 N.

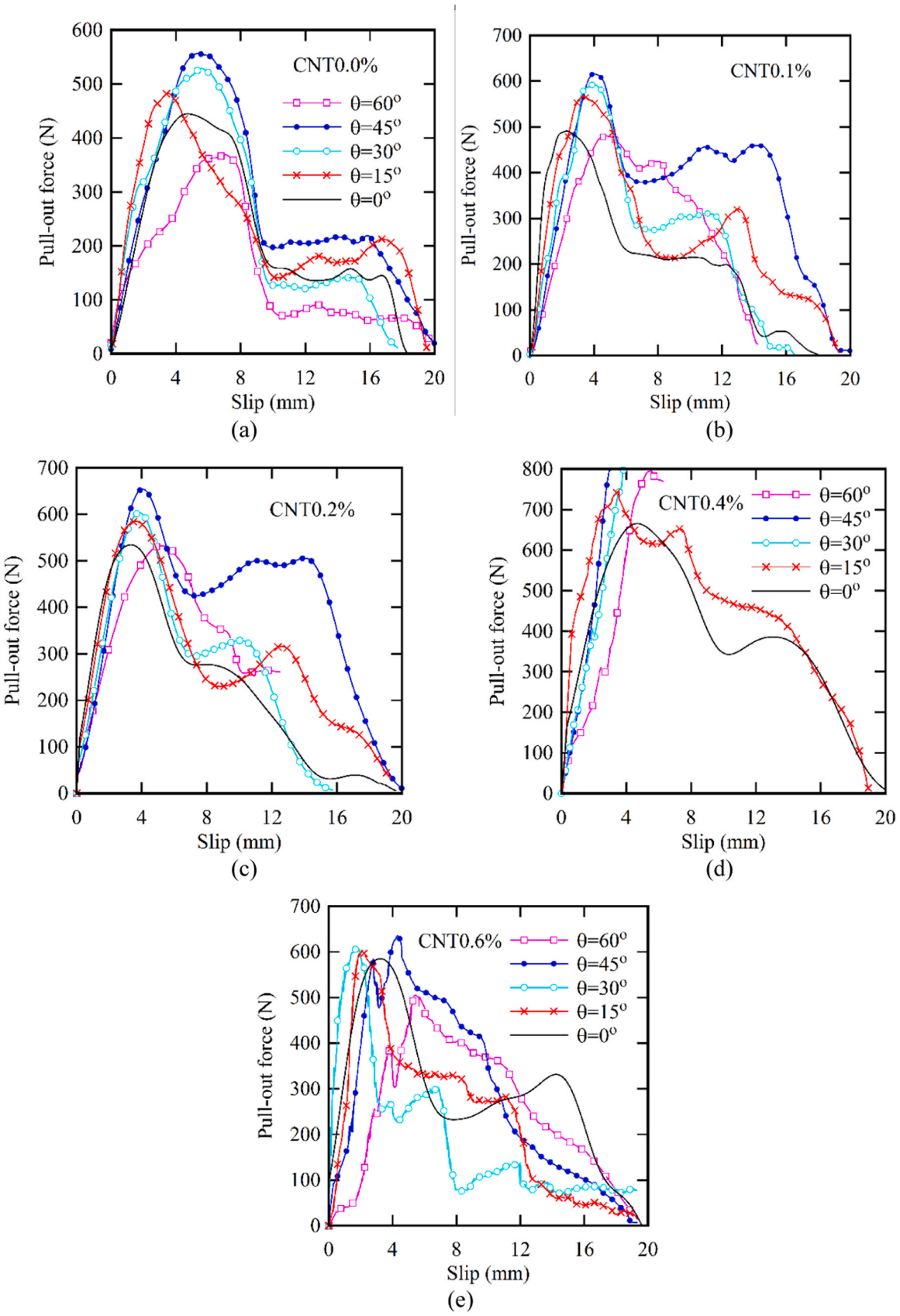

Fig. 15. Force-slip curves for UHPC samples containing 0 %, 0.1 %, 0.2 %, 0.4 %, and 0.6 % CNTs, with inclination angles of 0°, 15°, 30°, 45°, and 60°.

Table 6
Results for the maximum pull-out force, slip corresponding to the maximum force, pull-out energy, and fiber effectiveness.

	Inclination Angle (deg.)	Failure Mode	Peak Load (N)	Peak slip (mm)	Pull-out Work (kN.mm)	Bound Stress (MPa)	σ_{max}/f_u (%)
CNT−0.0 %	0	Pull-out	444.5	4.73	4.28	35.39	55.30
	15	Pull-out	482.3	6.51	4.77	38.40	60.00
	30	Pull-out	528.3	5.56	4.52	42.06	65.72
	45	Pull-out	556.3	5.36	5.49	44.29	69.21
	60	Pull-out	368.8	7.02	3.12	29.36	45.88
CNT−0.1 %	0	Pull-out	490.7	2.3	3.94	39.07	61.04
	15	Pull-out	566.6	3.32	5.28	45.11	70.49
	30	Pull-out	592.3	3.99	4.59	47.16	73.68
	45	Pull-out	615.8	4.01	7.07	49.03	76.61
	60	Pull-out	462.3	7.04	2.21	36.81	57.51
CNT−0.2 %	0	Pull-out	534.2	3.32	4.62	42.53	66.46
	15	Pull-out	587.7	3.61	5.88	46.79	73.11
	30	Pull-out	603.4	3.84	4.87	48.04	75.06
	45	Pull-out	654.3	4.05	8.31	52.09	81.40
	60	Pull-out	532.7	5.19	4.68	42.41	66.27
CNT−0.4 %	0	Pull-out	665.3	4.67	7.66	52.97	82.77
	15	Pull-out	782.6	2.04	3.82	62.31	97.36
	30	Rupture	800.2	3.92	1.47	63.71	100.00
	45	Rupture	800.2	3.01	1.08	63.71	100.00
	60	Rupture	800.2	5.55	2.05	63.71	100.00
CNT−0.6 %	0	Pull-out	585.9	3.22	6.31	46.65	72.89
	15	Pull-out	603.8	2.07	4.98	48.07	75.11
	30	Pull-out	612.6	1.68	4.06	48.77	76.21
	45	Pull-out	635.4	4.31	6.17	50.59	79.05
	60	Pull-out	505.5	5.42	5.39	40.25	62.89

and improving the mechanical engagement with concrete matrixes.

Table 6 demonstrates that increasing the CNT content improves the bond strength between the fibers and the UHPC matrix. In particular, the highest pull-out force values at inclination angle of 30°, 45°, and 60° were obtained in the 0.4 % CNT mix, and the fibers in this mix experienced rupture instead of pull-out. This indicates that the bond strength has increased to the point that the fibers fail before being pulled out. The relatively lower rupture force of hooked-end steel fibers observed in the finite element model results rather than theoretical rupture load, can be attributed to stress concentration effects at the curved hook regions of the fibers. These geometric discontinuities lead to localized intensification of stresses under tensile loading, which promotes earlier failure initiation compared to an idealized uniform fiber geometry. This phenomenon is captured in the numerical model and explains the lower rupture loads predicted compared to the theoretical tensile capacity based solely on nominal fiber strength and diameter. However, at 0.6 % CNT, the pull-out force decreased, which may be due to excessive agglomeration of the nanotubes and the creation of weak zones in the concrete. The amount of slip at the peak force is relatively large for mixes without CNTs, but this amount decreases with the addition of carbon nanotubes, indicating a reduction in plastic deformation before failure. The highest pull-out energy was recorded for the samples with 0.2 % CNT at inclination angle of 45°, which indicates increased energy absorption and improved mechanical connection performance. With an increase in CNTs to 0.4 %, the behavior of the samples changed from pull-out to rupture, which indicates an increase in adhesion to the point where the fibers tear instead of being pulled out. The bound stress value and the fiber efficiency ratio (σ_{max}/f_u) also increased with increasing CNT content and changing the fiber inclination angle. The highest value of this ratio was observed in the 0.4 % CNT samples at inclination angles of 30°, 45°, and 60°, which is a confirmation of the improved mechanical engagement of the fibers and increased adhesion resulting from the strengthening of the concrete matrix with carbon nanotubes.

An examination of the results table shows that the highest pull-out energy is associated with the CNT-0.2 % sample with inclination angle of 45°, the value of which is 8.31 kN·mm. This value indicates that, under these conditions, the appropriate combination of CNT content (0.2 %) and inclination angle (45°) resulted in the greatest energy absorption during the pull-out process. This may be due to a good balance between increasing the strength of the concrete and maintaining the mechanical adhesion of the fibers to the concrete matrix. In contrast, the lowest pull-out energy is associated with the CNT-0.4 % sample with a 45° inclination angle, the value of which is only 1.08 kN·mm. In this case, despite the increase in CNT content to 0.4 % and reaching the fiber rupture state, the amount of energy absorbed decreased. This decrease may be due to a change in the failure mechanism. In this case, instead of gradual pull-out, the fibers experience sudden rupture, and thus the overall energy absorbed is reduced. Overall, it is observed that increasing the CNT percentage to 0.2 % and an inclination angle of 45° leads to the greatest energy absorbed, but at higher CNT values, the failure mechanism changes, and the pull-out energy decreases.

4.5. Limitations and future directions

It is acknowledged that the number of specimens tested for each combination of CNT content and fiber inclination angle was limited to three, primarily due to the significant time and resource requirements associated with the preparation, curing, and testing of CNT-reinforced UHPC specimens. While triplicate testing and strict quality control were implemented to enhance the reliability and reproducibility of the results, the relatively small sample size may limit the statistical power and generalizability of the findings. Future studies are encouraged to employ larger sample sets to further validate the trends observed and to provide a more robust statistical analysis of the influence of CNT content and fiber orientation on the pull-out behavior in UHPC.

While this study successfully characterizes the mechanical pull-out behavior and fiber-matrix interaction in CNT-reinforced UHPC, it does not address the durability aspects of the composite under environmental exposures or long-term service conditions. Durability factors such as freeze-thaw resistance, chemical degradation, and fatigue behavior significantly influence the performance and lifespan of fiber-reinforced concretes. Future investigations should focus on evaluating the durability performance of CNT-enhanced UHPC, considering the effects of fiber orientation and CNT dispersion on the composite's resistance to environmental and mechanical deterioration. These studies will be essential for translating the mechanical improvements reported here into durable structural applications.

The dispersion of CNTs within the UHPC matrix was qualitatively ensured via ultrasonic agitation and visually assessed through SEM imaging. However, this study does not provide quantitative

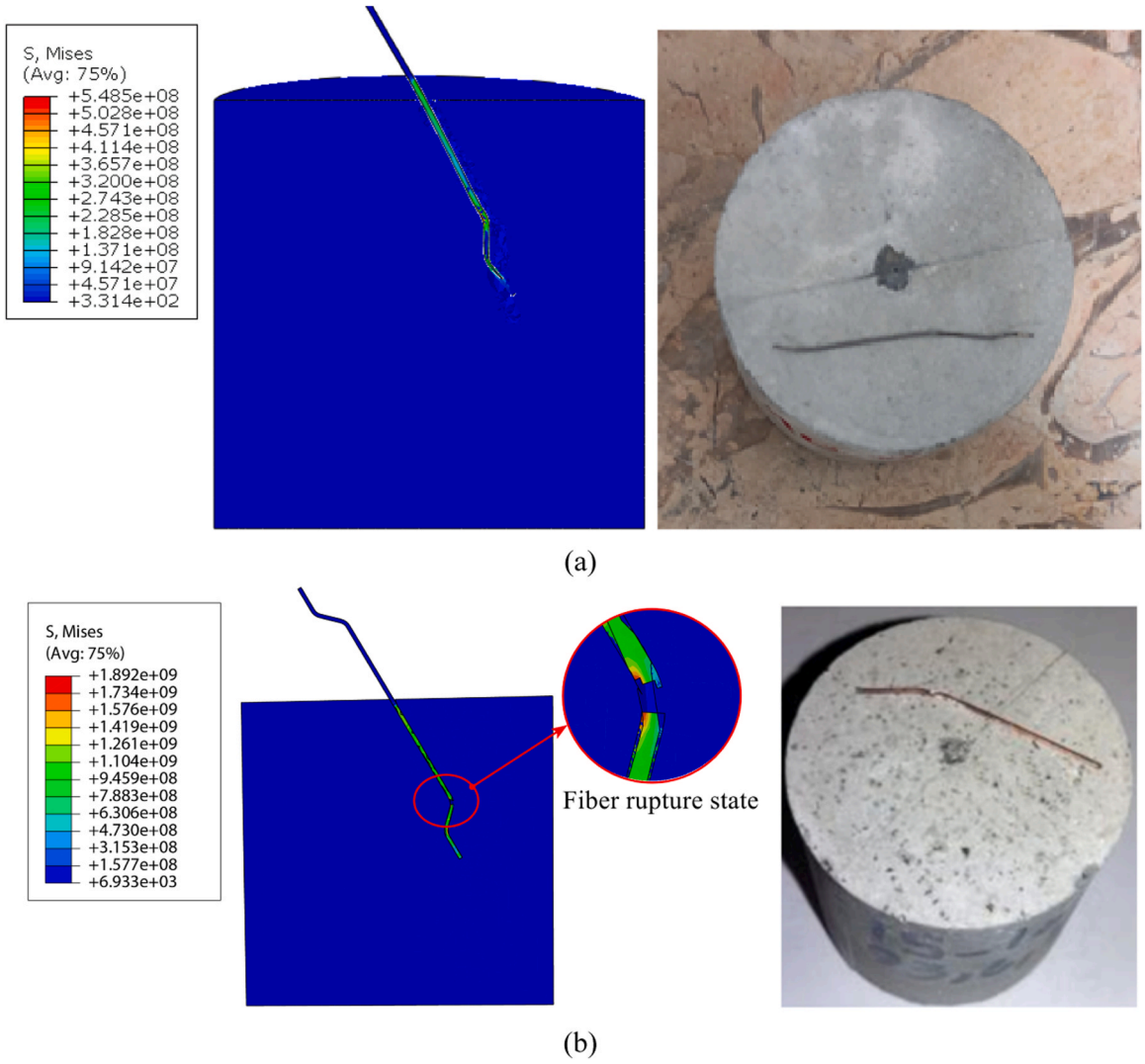

Fig. 16. Comparison between the von-Mises stress (Pa) of the fibers and their failure mechanism in the experimental tests and finite element simulations, (a) complete pull-out state (CNT-0.1 % with a 30° fiber inclination) and (b) fiber rupture state for (CNT-0.4 % with a 30° fiber inclination).

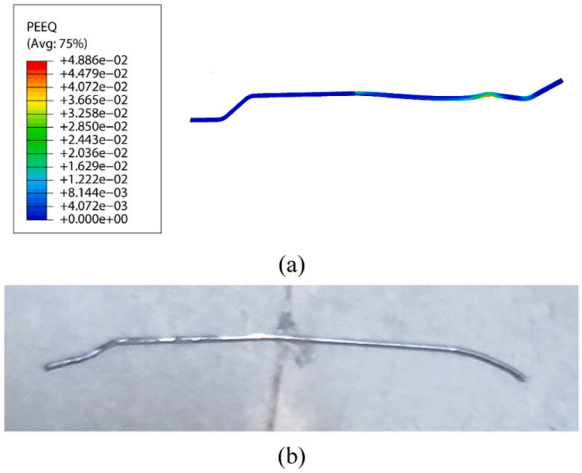

Fig. 17. Deformation of hooked-end steel fibers with a 45° inclination angle after being pulled out from UHPC containing 0.2 % CNT: (a) plastic strain distribution obtained from finite element modeling, (b) experimental fiber geometry after pull-out.

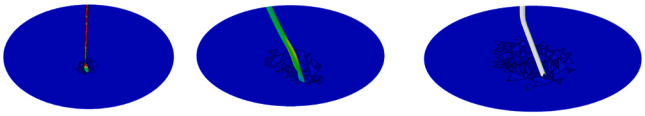

Fig. 18. Concrete failure mechanism in different samples.

measurements of dispersion homogeneity or agglomeration levels. Advanced characterization techniques such as Raman spectroscopy, image analysis, or rheological assessments were not employed but are recommended for future investigations. Quantifying CNT dispersion more rigorously will enhance understanding of its effects on mechanical properties and help optimize processing methods for CNT-reinforced UHPC.

5. Conclusion

This research investigated the influence of CNTs and the inclination angle of hooked-end steel fibers on the pull-out force, slip, pull-out energy, and failure mechanism in UHPC. This study advances the understanding of the synergistic effects of carbon nanotube reinforcement and fiber inclination on the pull-out behavior of hooked-end steel fibers in UHPC. The findings highlight how optimized CNT content and fiber

orientation significantly improve fiber-matrix adhesion, mechanical strength, and energy absorption. The validated finite element model offers a robust predictive framework that can support the design of UHPC composites with tailored mechanical properties, reducing experimental efforts and accelerating material optimization. The results showed that:

- The addition of CNT to UHPC improves fiber adhesion and increases the pull-out force. At a concentration of 0.4 %, the bond reaches its maximum, and fiber rupture occurs instead of pull-out. An inclination angle of 45° was determined to be the optimum angle for maximum pull-out force and energy absorption. However, at higher CNT contents (0.6 %), a relative decrease in the pull-out force was observed, likely due to the potential for creating weak zones and reducing the effectiveness of CNT dispersion.
- The inclination angle had a significant effect; the pull-out force increased up to an angle of 45° and then decreased, such that at an angle of 60°, the pull-out force was less than that at 0°.
- The finite element model with CZM parameters showed reasonable agreement with the laboratory results, but the predicted values were slightly higher than the experimental values.
- The highest pull-out energy was obtained at an inclination angle of 45° and a CNT content of 0.2 %, while at higher CNT percentages and specific angles, sudden fiber rupture occurred.
- Examination of the failure mechanism revealed that at low angles, gradual pull-out occurs, but at CNT percentages greater than 0.4 % and larger angles, fiber rupture was observed instead of controlled pull-out.

The addition of CNT to UHPC leads to a significant increase in pull-out strength that exceeds what can be explained solely by bulk matrix strengthening. CNTs enhance the fiber-matrix adhesion by improving nanoscale bonding and surface interactions, while simultaneously increasing fracture toughness by bridging microcracks and reducing matrix rupture. These effects contribute to higher peak pull-out forces, reduced slip, and increased energy absorption, sometimes causing a transition from fiber pull-out to fiber rupture. Physically, CNTs reinforce the matrix at the nanoscale by filling voids and bridging cracks, thereby improving load transfer and mechanical engagement between fibers and the concrete matrix. These insights demonstrate that CNTs not only strengthen the UHPC matrix but also play a critical role in enhancing fiber-matrix interfacial performance, which is essential for optimizing the durability and resilience of fiber-reinforced UHPC composites. These results are valuable for engineers and materials scientists aiming to enhance the performance, durability, and resilience of UHPC structural elements, ultimately contributing to the development of safer, more durable concrete infrastructure.

CRediT authorship contribution statement

Hakan Çağlar: Writing – review & editing, Writing – original draft, Visualization, Formal analysis, Data curation.

Declaration of Competing Interest

The authors declare that there are no conflicts of interest related to the publication of this article.

Data availability

No data was used for the research described in the article.

References

[1] G. Kravanja, A.R. Mumtaz, S. Kravanja, A comprehensive review of the advances, manufacturing, properties, innovations, environmental impact and applications of Ultra-High-Performance Concrete (UHPC), Buildings 14 (2) (2024) 382.
[2] X. Su, Z. Ren, P. Li, Review on physical and chemical activation strategies for ultra-high performance concrete (UHPC), Cem. Concr. Compos. (2024) 105519.
[3] X. Zhang, Z. Wu, J. Xie, X. Hu, C. Shi, Trends toward lower-carbon ultra-high performance concrete (UHPC)–a review, Constr. Build. Mater. 420 (2024) 135602.
[4] R. Piao, G.W. Kim, B. Chun, T. Oh, J.-W. Jeong, D.-Y. Yoo, Achieving thermoelectric properties of ultra-high-performance concrete using carbon nanotubes and fibers, Renew. Sustain. Energy Rev. 199 (2024) 114496.
[5] L.P. Prado, R. Carrazedo, M.K. El Debs, Interface strength of high-strength concrete to ultra-high-performance concrete, Eng. Struct. 252 (2022) 113591.
[6] M.K. Al-Madani, M.A. Al-Osta, S. Ahmad, H.R. Khalid, M. Al-Huri, Interfacial bond behavior between ultra high performance concrete and normal concrete substrates, Constr. Build. Mater. 320 (2022) 126229.
[7] C. Lin, T. Kanstad, S. Jacobsen, G. Ji, Bonding property between fiber and cementitious matrix: a critical review, Constr. Build. Mater. 378 (2023) 131169.
[8] I. Sharifi, M.H. Sherzai, A. Javanmard, F. Yalçındağ, İ. Özgür Yaman, Uniaxial tensile performance in the warp and weft directions of carbon textile reinforced concretes with two different matrices, Constr. Build. Mater. 476 (2025) 141292.
[9] J. Esmaeili, I. Sharifi, K. Andalibi, J. Kasaei, Effect of different matrix compositions and micro steel fibers on tensile behavior of textile reinforced concrete, in: IOP Conference Series: Materials Science and Engineering, IOP Publishing, 2017.
[10] X. Kong, Y. Yao, B. Wu, W. Zhang, W. He, Y. Fu, The impact resistance and mechanical properties of recycled aggregate concrete with hooked-end and crimped steel fiber, Materials 15 (19) (2022) 7029.
[11] G. Laxmi, S. Patil, N. Hossiney, H. Thejas, Effect of hooked end steel fibers on strength and durability properties of ambient cured geopolymer concrete, Case Stud. Constr. Mater. 18 (2023) e02122.
[12] Y. Huang, J. Huang, W. Zhang, X. Liu, Experimental and numerical study of hooked-end steel fiber-reinforced concrete based on the meso-and macro-models, Compos. Struct. 309 (2023) 116750.
[13] M. Pirani, M. Hahn, H.D. Joghan, A.E. Tekkaya, S. Farahani, On the potential of manufacturing multi-material components with micro/nanocellular structures via the hybrid process of electromagnetic forming injection foaming, J. Micro Nano Sci. Eng. 12 (3) (2024).
[14] Y. Yu, G. Zhu, Q. Zhang, M. Behzadnia, Z. Yang, Y. Liu, J. Xie, Multinonmetal-doped V2O5 nanocomposites for lithium-ion battery cathodes, ACS Appl. Energy Mater. 7 (23) (2024) 11031–11037.
[15] M. Hoseinzadeh, R. Pilafkan, V.A. Maleki, Size-dependent linear and nonlinear vibration of functionally graded CNT reinforced imperfect microplates submerged in fluid medium, Ocean Eng. 268 (2023) 113257.
[16] P. Vahidi Pashaki, M. Pouya, V.A. Maleki, High-speed cryogenic machining of the carbon nanotube reinforced nanocomposites: finite element analysis and simulation, Proceedings Institution Mechanical Engineers Part C Journal Mechanical Engineering Science 232 (11) (2018) 1927–1936.
[17] M. Minaei, M. Rezaee, V. Arab Maleki, Vibration analysis of viscoelastic carbon nanotube under electromagnetic fields based on the nonlocal Timoshenko beam theory, Iran. J. Mech. Eng. Trans. ISME 23 (2) (2021) 176–198.
[18] V. Gharebagh, G. Rezazadeh, N. Sharafkhani, R. Shabani, Static and dynamic response of carbon nanotube-based nano-tweezers, Int. J. Eng. 24 (4) (2011) 377–386.
[19] V. Anish, J. Logeshwari, A review on ultra high-performance fibre-reinforced concrete with nanomaterials and its applications, J. Eng. Appl. Sci. 71 (1) (2024) 25.
[20] G. Murali, S.R. Abid, M. Amran, R. Fediuk, N. Vatin, M. Karelina, Combined effect of multi-walled carbon nanotubes, steel fibre and glass fibre mesh on novel two-stage expanded clay aggregate concrete against impact loading, Crystals 11 (7) (2021) 720.
[21] G. Xing, Y. Xu, J. Huang, Y. Lu, P. Miao, P. Chindasiriphan, P. Jongvivatsakul, K. Ma, Research on the mechanical properties of steel fibers reinforced carbon nanotubes concrete, Constr. Build. Mater. 392 (2023) 131880.
[22] Y. Liu, Y. Huang, Analytic solution of pull-out failure on bond-slip relationship between deformed rebar and ultra-high-performance concrete, Eng. Struct. 305 (2024) 117682.
[23] X.-L. Gao, S.-Y. Shen, Y. Wan, S.-W. Qin, Experimental study on bond behavior of steel bar embedded in thin UHPC, J. Build. Eng. 86 (2024) 108865.
[24] P. Zhao, X. Shao, J. Cao, X. Rong, Experimental research on pull-out behavior of steel-UHPC composite beams with new composite dowels connectors, Eng. Struct. 312 (2024) 118182.
[25] L. Zhang, J. Zhao, C. Fan, Z. Wang, Effect of surface shape and content of steel fiber on mechanical properties of concrete, Adv. Civ. Eng. 2020 (1) (2020) 8834507.
[26] C.Y. Li, B. Mobasher, Finite element simulations of fiber pullout toughening in fiber reinforced cement based composites, Adv. Cem. Based Mater. 7 (3-4) (1998) 123–132.
[27] S.H. Lee, S. Kim, D.-Y. Yoo, Hybrid effects of steel fiber and carbon nanotube on self-sensing capability of ultra-high-performance concrete, Constr. Build. Mater. 185 (2018) 530–544.
[28] J. Esmaeili, K. Andalibi, O. Gencel, F.K. Maleki, V.A. Maleki, Pull-out and bond-slip performance of steel fibers with various ends shapes embedded in polymer-modified concrete, Constr. Build. Mater. 271 (2021) 121531.
[29] J. Esmaeili, K. Andalibi, O. Gencel, Mechanical characteristics of experimental multi-scale steel fiber reinforced polymer concrete and optimization by Taguchi methods, Constr. Build. Mater. 313 (2021) 125500.

[30] J. Esmaeili, V. Romouzi, J. Kasaei, K. Andalibi, An investigation of durability and the mechanical properties of ultra-high performance concrete (UHPC) modified with economical graphene oxide nano-sheets, J. Build. Eng. 80 (2023) 107908.
[31] M. Pouraminian, A.E. Akbari Baghal, K. Andalibi, F. Khosravi, V. Arab Maleki, Enhancing the pull-out behavior of ribbed steel bars in CNT-modified UHPFRC using recycled steel fibers from waste tires: a multiscale finite element study, Sci. Rep. 14 (1) (2024) 19939.
[32] D.-Y. Yoo, S. Kim, J.-J. Kim, B. Chun, An experimental study on pullout and tensile behavior of ultra-high-performance concrete reinforced with various steel fibers, Constr. Build. Mater. 206 (2019) 46–61.
[33] P.A. Krahl, Gd.M.S. Gidrão, R.B. Neto, R. Carrazedo, Effect of curing age on pullout behavior of aligned and inclined steel fibers embedded in UHPFRC, Constr. Build. Mater. 266 (2021) 121188.
[34] X. Wang, Y. Liu, D.-Y. Yoo, Combined corrosion and inclination effects on pullout behavior of various steel fibers under wet-dry cycle deterioration, Cem. Concr. Compos. 142 (2023) 105229.
[35] H. Li, F. Liu, Y. Li, X. Li, Y. Pan, C. Liu, Effects of fiber spacing and inclination on the pull-out behaviors of arc-shaped fibers in brittle SIFCON matrix, Constr. Build. Mater. 419 (2024) 135381.
[36] S.W. Lee, G.W. Kim, T. Oh, I. You, X. Wang, D.-Y. Yoo, The microstructure and mechanical properties of cementless ultra-high-performance alkali activated concrete considering geometrical properties of steel fiber, Cem. Concr. Compos. 142 (2023) 105209.
[37] Y.Y.Y. Cao, Q.L. Yu, Effect of inclination angle on hooked end steel fiber pullout behavior in ultra-high performance concrete, Compos. Struct. 201 (2018) 151–160.
[38] Y. Lee, S.-T. Kang, J.-K. Kim, Pullout behavior of inclined steel fiber in an ultra-high strength cementitious matrix, Constr. Build. Mater. 24 (10) (2010) 2030–2041.
[39] J.-J. Kim, D.-Y. Yoo, Effects of fiber shape and distance on the pullout behavior of steel fibers embedded in ultra-high-performance concrete, Cem. Concr. Compos. 103 (2019) 213–223.
[40] B.A. Graybeal, Characterization of the Behavior of Ultra-high Performance Concrete, University of Maryland, College Park, 2005.
[41] S.-J. Lee, D.-Y. Yoo, D.-Y. Moon, Effects of hooked-end steel fiber geometry and volume fraction on the flexural behavior of concrete pedestrian decks, Appl. Sci. 9 (6) (2019) 1241.
[42] X. Wang, B. Xu, K. Luan, R. Mu, J. Chen, Optimization of the shape of hooked-end steel fiber based on pulling out and reinforcing cementitious composites, Materials 17 (1) (2023) 47.
[43] U. Kalwane, Y. Ghugal, A. Dahake, Toughness of polymer modified steel fiber reinforced concrete, Open J. Civ. Eng. 6 (1) (2016) 8–18.
[44] N. Sharafkhani, A Helmholtz resonator-based acoustic metamaterial for power transformer noise control, Acoust. Aust. 50 (1) (2022) 71–77.
[45] N. Sharafkhani, An ultra-thin multi-layered metamaterial for power transformer noise absorption, Build. Acoust. 29 (1) (2022) 53–62.
[46] J. Guan, B. Zhang, C. Xie, L. Li, M. Khan, Meso-fracture model of ultra-high-performance fiber-reinforced geopolymer concrete pertinent to aggregate gradation and fiber spacing, Eng. Fract. Mech. (2025) 110877.
[47] A. Qasem, Y.S. Sallam, H. Hossam Eldien, B.H. Ahangarn, Bond-slip behavior between ultra-high-performance concrete and carbon fiber reinforced polymer bars using a pull-out test and numerical modelling, Constr. Build. Mater. 260 (2020) 119857.
[48] Z.-J. Wang, Y.-X. Ban, W.-Y. Luo, H.-X. Fan, B. Zhang, L.-M. Wu, S.-C. Wang, Analysis of flexural bearing capacity and failure mode of precast LSFRC pavement slab, Adv. Mater. Sci. Eng. 2022 (1) (2022) 2528085.
[49] A. Pourasghar, E. Mehdizadeh, T.C. Wong, A.K. Hoskoppal, J.C. Brigham, A computationally efficient approach for estimation of tissue material parameters from clinical imaging data using a level set method, J. Eng. Mech. 150 (10) (2024) 04024075.
[50] A.E.A. Baghal, A. Maleki, R. Vafaei, On the pull-out behavior of hooked-end shape memory alloys fibers embedded in ultra-high performance concrete, Int. J. Eng. Technol. Innov. 11 (4) (2021).
[51] A.E. Akbari Baghal, A. Maleki, R. Vafaeipour Sorkhabi, Finite element analysis of the adhesive behavior of shape memory alloy fiber and polymer concrete, J. Sci. Technol. Compos. 7 (4) (2021) 1255–1262.